2842 *Chem. Mater.* **2010,** *22,* 2842–2849
DOI:10.1021/cm100010z

CHEMISTRY OF MATERIALS
Article

$Sr_{2.975-x}Ba_xCe_{0.025}AlO_4F$: a Highly Efficient Green-Emitting Oxyfluoride Phosphor for Solid State White Lighting

Won Bin Im,* Stuart Brinkley, Jerry Hu, Alexander Mikhailovsky, Steven P. DenBaars, and Ram Seshadri

Solid State Lighting and Energy Center, Materials Department, Department of Chemistry and Biochemistry, and Materials Research Laboratory, University of California, Santa Barbara, California 93106

Received January 3, 2010. Revised Manuscript Received March 17, 2010

A new, highly efficient green oxyfluoride phosphor family $Sr_{2.975-x}Ba_xCe_{0.025}AlO_4F$ (SBAF:Ce^{3+}) has been developed as a component of solid state white light emitting diodes (LED). The phosphor emits with a maximum at 502 nm when excited by 405 nm excitation, with a quantum efficiency approaching 100%. When SBAF:Ce^{3+} ($x = 1.0$) is incorporated with encapsulant on an ultraviolet (405 nm) LED, greenish-white light with a color rendering index of 62 under a forward bias current of 20 mA is obtained. The results suggest that phosphors deriving from SBAF:Ce^{3+} have potential for incorporation in formulations for white LEDs and related applications. The preparation and structural and optical characterization of the phosphor family is described. Attempts to understand the origins of the high efficiency on the basis of the thermal quenching characteristics of SBAF:Ce^{3+} in comparison with related compounds are presented.

Introduction

Continuing improvement in the efficiency of light emitting diodes (LED) has provided the potential for tremendous energy saving in general lighting applications: LEDs currently possess between 2 and 10 times the efficiency of incandescent and fluorescent lamps.[1−3] LEDs can therefore play a significant role in combating global warming through reducing energy consumption.[4] Because of their reduced power use, LEDs in conjunction with renewable energy sources also offer great promise in addressing lighting in remote and underdeveloped areas of the world. Toward these ends, the Optoelectronics Industry Development Association (OIDA) plans to achieve 200 lm/W efficacy with good color rendering by 2020.[5] To achieve this goal, new phosphors with high efficiency are key, since the eventual performance of white GaN-LED based devices depends strongly on the phosphor.[6−9] The most frequently used yellow phosphor is garnet $Y_3Al_5O_{12}$:Ce^{3+} (YAG:Ce^{3+}). It is highly efficient under blue excitation, and has been studied by many groups[10,11] since its development in 1967 by Blasse and Bril.[12,13] Other new and promising phosphors include a host of nitrides and oxynitrides from the groups of Schnick, Hintzen, and Mitomo,[14−21] oxysulfides,[22] garnets,[23−25] and vanadate solid solutions.[26]

Recently we reported a new yellow-emitting phosphor $LaSr_2AlO_5$:Ce^{3+} (LSA:Ce^{3+}),[9,27] potentially applicable to white LED assemblies. $LaSr_2AlO_5$ is isostructural with

*To whom correspondence should be addressed. E-mail: imwonbin@mrl.ucsb.edu.

(1) Pimputkar, S.; Speck, J. S.; DenBaars, S. P.; Nakamura, S. *Nat. Photonics* **2009**, *3*, 179.
(2) Schubert, E. F.; Kim, J. K. *Science* **2005**, *308*, 1274.
(3) Hashimoto, T.; Wu, F.; Speck, J. S.; Nakamura, S. *Nat. Mater.* **2007**, *6*, 568.
(4) Nakamura, S. *MRS Bull.* **2009**, *34*, 101.
(5) Allen, S. C.; Steckl, A. J. *Appl. Phys. Lett.* **2008**, *92*, 1433091.
(6) Im, W. B.; Fellows, N. N.; DenBaars, S. P.; Seshadri, R. *J. Mater. Chem.* **2009**, *19*, 1325.
(7) Yang, Y. C.; Wang, S. L. *J. Am. Chem. Soc.* **2008**, *130*, 1146.
(8) Ki, W.; Li, J. *J. Am. Chem. Soc.* **2008**, *130*, 8114.
(9) Im, W. B.; Kim, Y. I.; Fellows, N. N.; Masui, H.; Hirata, G. A.; DenBaars, S. P.; Seshadri, R. *Appl. Phys. Lett.* **2008**, *93*, 0919051.
(10) Tien, T. Y.; Gibbons, E. F.; Delosh, R. G.; Zacmanid, P. J.; Smith, D. E.; Stadler, H. L. *J. Electrochem. Soc.* **1973**, *120*, 278.
(11) Nyman, M.; Shea-Rohwer, L. E.; Martin, J. E.; Provencio, P. *Chem. Mater.* **2009**, *21*, 1536.
(12) Blasse, G.; Bril, A. *Appl. Phys. Lett.* **1967**, *11*, 53.
(13) Jang, H. S.; Im, W. B.; Lee, D. C.; Jeon, D. Y.; Kim, S. S. *J. Lumin.* **2007**, *126*, 371.
(14) Bachmann, V.; Ronda, C.; Oeckler, O.; Schnick, W. *Chem. Mater.* **2009**, *21*, 316.
(15) Kechele, J. A.; Hecht, C.; Oeckler, O.; auf der Günne, J. S.; Schmidt, P. J.; Schnick, W. *Chem. Mater.* **2009**, *21*, 1288.
(16) Hecht, C.; Stadler, F.; Schmidt, P. J.; auf der Günne, J. S.; Baumann, V.; Schnick, W. *Chem. Mater.* **2009**, *21*, 1595.
(17) Zeuner, M.; Schmidt, P. J.; Schnick, W. *Chem. Mater.* **2009**, *21*, 2467.
(18) Li, Y. Q.; Delsing, A. C. A.; de With, G.; Hintzen, H. T. *Chem. Mater.* **2005**, *17*, 3242.
(19) Li, Y. Q.; Delsing, A. C. A.; de With, G.; Hintzen, H. T. *Chem. Mater.* **2005**, *17*, 7.
(20) Xie, R. J.; Hirosaki, N.; Sakuma, K.; Yamamoto, Y.; Mitomo, M. *Appl. Phys. Lett.* **2004**, *84*, 5404.
(21) Suehiro, T.; Hirosaki, N.; Xie, R. J.; Mitomo, M. *Chem. Mater.* **2005**, *17*, 308.
(22) Kawahara, Y.; Petrykin, V.; Ichihara, T.; Kijima, N.; Kakihana, M. *Chem. Mater.* **2006**, *18*, 6303.
(23) Gundiah, G.; Shimomura, Y.; Kijima, N.; Cheetham, A. K. *Chem. Phys. Lett.* **2008**, *455*, 279.
(24) Setlur, A. A.; Heward, W. J.; Gao, Y.; Srivastava, A. M.; Chandran, R. G.; Shankar, M. V. *Chem. Mater.* **2006**, *18*, 3314.
(25) Setlur, A. A.; Heward, W. J.; Hannah, M. E.; Happek, U. *Chem. Mater.* **2008**, *20*, 6277.
(26) Neeraj, S.; Kijima, N.; Cheetham, A. K. *Solid State Commun.* **2004**, *131*, 65.
(27) Im, W. B.; Fellows, N. N.; DenBaars, S. P.; Seshadri, R.; Kim, Y.-I. *Chem. Mater.* **2009**, *21*, 2957.

 Published on Web 03/30/2010

the oxyfluoride Sr_3AlO_4F (SAF) reported previously by Kennedy, Woodward, and co-workers.[28−30] Solid solution is possible between the LSA and SAF compounds, and a preliminary study on the substitution of F^- for O^{2-}, compensated by Sr^{2+} for Gd^{3+} in the phosphor host $GdSr_2AlO_5$:Ce^{3+} has been made by us.[31] In this study, we report two substitutions, both of anions (F for O) and of cations (Ba for Sr) that result in the oxyfluoride phosphor family $Sr_{2.975-x}Ba_xCe_{0.025}AlO_4F$ (SBAF:Ce^{3+}), describing structure, using a combination of powder X-ray diffraction (XRD) and 2D ^{19}F NMR spectroscopy, and optical properties. The use of NMR is important since diffraction techniques do not easily distinguish O and F. Optical property measurements show that SBAF:Ce^{3+} is a very bright, broad, emitter under 400 nm excitation. White LEDs based on a combination of an InGaN LED chip (λ_{max} = 405 nm) with the SBAF:Ce^{3+} phosphors have been fabricated and are discussed. Thermal quenching of the luminescence, and in particular, comparison of the behavior of SBAF:Ce^{3+} with the parent $LaSr_2AlO_5$:Ce^{3+} compound suggest reasons for the unusual brightness of the new phosphor.

Experimental Section

Powder samples of $Sr_{3-x-y}Ba_xCe_yAlO_4F$ (SBAF:Ce^{3+}, x = 0 and 1.0) were prepared by solid-state reaction from $SrCO_3$ (Aldrich, 99.995%), SrF_2 (Aldrich, 99.9%), $BaCO_3$ (Alfa, 99.99%), BaF_2 (Aldrich, 99.99%), Al_2O_3 (Aldrich, 99.9%), and CeO_2 (Aldrich, 99.9%). The concentration of Ce was optimized at 0.025 atom % in the formula unit. The powder reagents were intimately ground together and heated at 1400 °C in a reducing atmosphere of H_2/N_2 (5%/95%) for 4 h. Powder XRD data were obtained using Cu−Kα radiation (Philips X'Pert) over the angular range 20° ≤ 2θ ≤ 100° with a step size of 0.016°. Crystal structure refinement employed the Rietveld method as implemented in the General Structure Analysis System (GSAS) software suite.[32] Magic angle spinning (MAS) NMR experiments were carried out on a Bruker AVANCE 500 MHz WB spectrometer, operated at 470.6 MHz for ^{19}F-NMR. Room temperature photoluminescence (PL) spectra were measured on a Perkin-Elmer LS55 luminescence spectrophotometer scanning the wavelength range of 300 to 700 nm. Quantum efficiency (QE) was measured with 405 nm excitation using an argon laser and a setup as described by Greenham et al.[33] Details of the QE measurements are provided in the Supporting Information.

Prototype LED devices were fabricated by applying an intimate mixture of SBAF:Ce^{3+} and transparent silicone resin on a InGaN LED (λ_{max} = 405 nm). For electroluminescence measurements, discrete LEDs grown on *m*-plane GaN[34] were placed on silver headers, and gold wires were attached for electrical operation. The device was then encapsulated in a phosphor/silicone mixture, with the mixture placed directly on headers, and then cured. After packaging was completed, the device with phosphor was measured in an integrating sphere under direct current (DC) bias forward conditions.

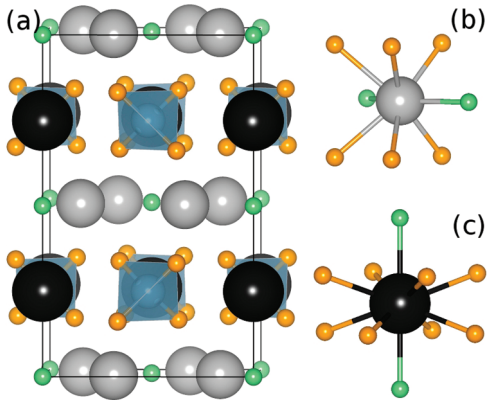

Figure 1. (a) Unit cell representation of the fully ordered crystal structure of Sr_2BaAlO_4F (SBAF). Light gray, dark gray, blue, orange, and green spheres represent Sr, Ba, Al, O, and F atoms, respectively. The polyhedral geometry of (b) SrO_6F_2 at 8*h* (x, $x+{}^1/_2$, 0) and (c) BaO_8F_2 at 4*a* (0, 0, ${}^1/_4$) are depicted.

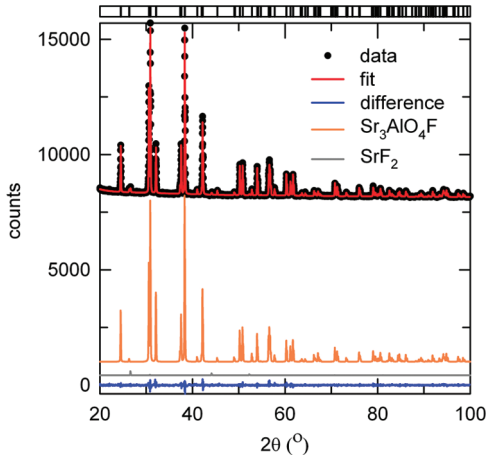

Figure 2. Rietveld refinement of the powder XRD profile of $Sr_{2.975}Ce_{0.025}AlO_4F$. Expected reflection positions are displayed using vertical lines. A second SrF_2 impurity phase (4.6 wt %) was included in the refinement, and contributions from the two phases to the fit are depicted.

Results

Figure 1 displays the unit cell representation of SBAF. The 8*h* and 4*a* sites in this structure are fully occupied by Sr and Ba, respectively, and the 4*b* site is occupied by Al. F is believed to occupy the 4*c* site and the 16*l* site is occupied by O. Sr and Ba sites corresponding to polyhedra with 8-coordination (Sr) and 10-coordination (Ba) are both substituted by Ce ions. Both SrO_6F_2 and BaO_8F_2 polyhedra comprise two F atoms and six or eight (respectively) O atoms. Structurally SBAF belongs to the Cs_3CoCl_5-family (tetragonal, space group *I*4/*mcm*),[35] and is also closely related to $Ba_3M^{4+}O_5$-type compounds (tetragonal, space group *P*4/*ncc*).[36]

Figure 2 displays the results of Rietveld refinement of the XRD data profiles of SBAF:Ce^{3+} (x = 0). A small

(28) Vogt, T.; Woodward, P. M.; Hunter, B. A.; Prodjosantoso, A. K.; Kennedy, B. J. *J. Solid State Chem.* **1999**, *144*, 228.
(29) Prodjosantoso, A. K.; Kennedy, B. J.; Vogt, T.; Woodward, P. M. *J. Solid State Chem.* **2003**, *172*, 89.
(30) Park, S.; Vogt, T. *J. Lumin.* **2009**, *129*, 952.
(31) Im, W. B.; Fourré, Y.; Brinkley, S.; Sonoda, J.; Nakamura, S.; DenBaars, S. P.; Seshadri, R. *Opt. Express* **2009**, *17*, 22673.
(32) Larson, A. C.; Von Dreele, R. B. *General Structure Analysis System (GSAS)*; Los Alamos National Laboratory Report LAUR 86-748; Los Alamos National Laboratory: Los Alamos, NM, 1994.
(33) Greenham, N. C.; Samuel, I. D. W.; Hayes, G. R.; Phillips, R. T.; Kessener, Y. A. R. R.; Moratti, S. C.; Holmes, A. B.; Friend, R. H. *Chem. Phys. Lett.* **1995**, *241*, 89.
(34) Schmidt, M. C.; Kim, K. C.; Sato, H.; Fellows, N.; Masui, H.; Nakamura, S.; DenBaars, S. P.; Speck, J. S. *Jpn. J. Appl. Phys.* **2007**, *46*, L126.
(35) Drofenik, M.; Golic, L. *Acta Crystallogr.* **1979**, *B35*, 1059.
(36) Dent, L. S.; Glasser, F. P. *Acta Crystallogr.* **1965**, *18*, 453.

Table 1. Structural Parameters of $Sr_{2.975}Ce_{0.025}AlO_4F$ and $Sr_{1.975}Ba_{Ce0.025}AlO_4F$ as Determined by the Rietveld Refinement of Powder XRD Data at Room Temperature

atom	site	x	y	z	U_{iso} (Å^2)
		$Sr_{2.975}Ce_{0.025}AlO_4F$[a]			
Sr1	8*h*	0.1685(1)	$x + {}^1/_2$	0	0.0121(2)
Sr2	4*a*	0	0	${}^1/_4$	0.0188(6)
Al	4*b*	0	${}^1/_2$	${}^1/_4$	0.0131(2)
F	4*c*	0	0	0	0.0229(3)
O	16*l*	0.1424(4)	$x + {}^1/_2$	0.6485(7)	0.0247(9)
		$Sr_{1.975}BaCe_{0.025}AlO_4F$[b]			
Sr1	8*h*	0.1690(6)	$x + {}^1/_2$	0	0.0130(3)
Ba1	4*a*	0	0	${}^1/_4$	0.0176(3)
Al	4*b*	0	${}^1/_2$	${}^1/_4$	0.0321(2)
F	4*c*	0	0	0	0.0009(1)
O	16*l*	0.1396(5)	$x + {}^1/_2$	0.6461(6)	0.0798(4)

[a] Space group: *I*4/*mcm* (No.140), $Z = 4$, $a = b = 6.7720(1)$ Å, $c = 11.1485(2)$ Å, $V = 511.2(1)$ Å^3. [b] Space group: *I*4/*mcm* (No.140), $Z = 4$, $a = b = 6.9189(6)$ Å, $c = 11.2071(7)$ Å, $V = 536.5(6)$ Å^3.

Table 2. Select Distances and Bond Valence Sums (BVS) Found in $Sr_{2.975}Ce_{0.025}AlO_4F$ and $Sr_{1.975}BaCe_{0.025}AlO_4F$

	distance (Å)	atom	BVS
	$Sr_{2:975}Ce_{0:025}AlO_4F$		
Sr1−O	(2×) 2.454(5)	Sr1	2.2
	(4×) 2.685(4)	Sr2	1.4
Sr1−F	(2×) 2.518(2)		
Sr2−O	(8×) 2.841(4)		
Sr2−F	(2×) 2.787(1)		
	$Sr_{1.975}BaCe_{0.025}AlO_4F$		
Sr1−O	(2×) 2.452(2)	Sr1	2.0
	(4×) 2.731(3)	Ba1	1.9
Sr1−F	(2×) 2.572(2)		
Ba1−O	(8×) 2.891(1)		
Ba1−F	(2×) 2.801(4)		

impurity of SrF_2 (4.6 wt %) was included in the refinement. The compound is tetragonal in space group *I*4/*mcm* (S.G. #140), and the cell parameters are $a = b = 6.7720(1)$ Å $c = 11.1485(2)$ Å. Structural parameters, selected interatomic distances, and bond valence sums (BVS) are listed in Table 1 and Table 2, respectively. The BVS for the structure refinement of SBAF:Ce^{3+} ($x = 0$) suggest that Sr2 is somewhat underbonded with BVS = 1.4, while Sr1 has BVS = 2.2 (see Table 2). Figure 3 displays the results of Rietveld profile refinement for SBAF:Ce^{3+} ($x = 1.0$), obtained with goodness of fit parameters $R_{wp} = 3.49\%$ and $\chi^2 = 1.37$. Compared with the Ba-free composition ($x = 0$), the tetragonal cell parameters of SBAF:Ce^{3+} ($x = 1.0$) increase in agreement with the ionic radius of Ba^{2+} being larger than that of Sr^{2+}. From the BVS results on the Ba-free composition ($x = 0$), we can expect that the site preference of Ba is likely to be for the 4*a* site, and this substitution stabilizes the SAF compound in agreement with prior work.[29] This is indeed borne out from the BVS listed in Table 1. It should be noted here that all bond valence calculations assume complete ordering of O and F as described earlier.

We note that as formulated, the compositions $Sr_{2.975-x}Ba_xCe_{0.025}AlO_4F$ are not charge balanced, and have a slight excess of positive charge (0.025 in the formula) because of Ce^{3+} substituting Sr^{2+} and Ba^{2+}. The structure offers many mechanisms to compensate this excess

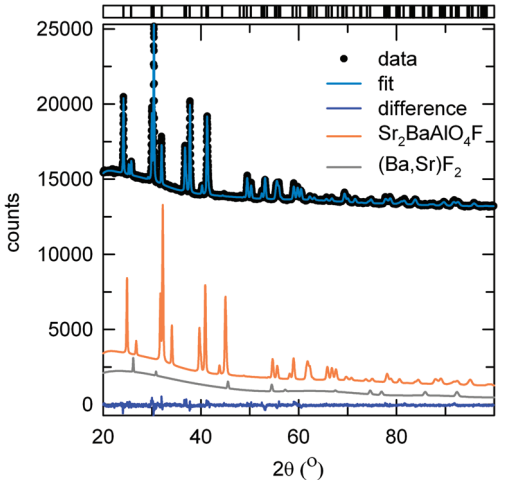

Figure 3. Rietveld refinement of the powder XRD profile of $Sr_{1.975}BaCe_{0.025}AlO_4F$. Expected reflection positions are displayed using vertical lines. A second $(Ba/Sr)F_2$ impurity phase (4.2 wt %) was included in the refinement, and contributions from the two phases to the fit are depicted.

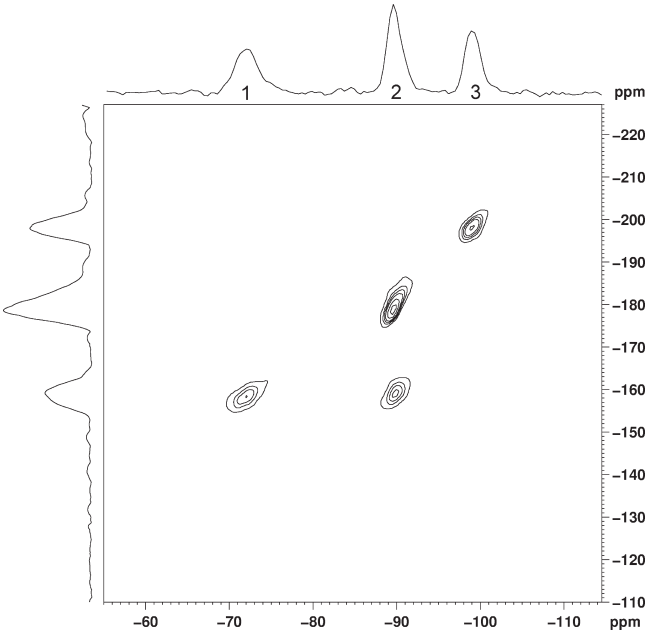

Figure 4. ^{19}F BABA 2D MAS NMR of $Sr_{1.975}BaCe_{0.025}AlO_4F$. The single and double quantum dimensions are displayed as abscissa and ordinate, respectively. The resonance marked 3 is due to the $(Ba,Sr)F_2$ impurity and is uncorrelated with the resonances 1 and 2 that arise from F distributing over two sites in the SAF structure. The resonances 1 and 2 are correlated but weak 1−1 correlations (absence of intensity adjacent to 1 on the diagonal) which suggests that the F at site 1 is relatively sparsely populated, unlike at 2. Chemical shifts are referenced to $CFCl_3$.

charge, the most obvious being slight off-stoichiometry between F and O, with a slight excess of the latter. Since the experimental techniques we have employed here, namely, optical properties, Rietveld refinement of powder X-ray diffraction data, and ^{19}F NMR spectroscopy, are not sensitive to substitutions at this level, we present the formula for the title compounds as written, in preference to speculation.

The location of fluorine in SBAF:Ce^{3+} is crucial to understand the optical properties of the phosphors. Oxygen and fluorine are neighboring atoms in the periodic

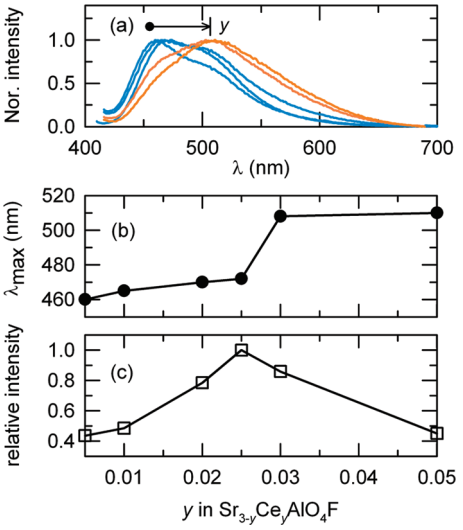

Figure 5. (a) Emission spectra of $Sr_{3-y}Ce_yAlO_4F$ under 400 nm excitation source with varying Ce^{3+} concentration y. (b) Position of the emission maximum and (c) relative emission intensity as a function of Ce^{3+} substitution y.

table, and O^{2-} and F^- have no contrast in X-ray scattering. Coincidentally, their coherent neutron scattering lengths are also within 3% of each other. As a consequence, crystallographic studies of O/F ordering are difficult to undertake. As an alternative analytical tool, solid-state NMR spectroscopy provides a powerful probe of ^{19}F for studying oxygen/fluorine ordering in disordered systems. The ^{19}F BABA (back-to-back) MAS NMR spectrum[37] of SBAF:Ce^{3+} show two resonance peaks appearing at −72 ppm (labeled 1) and −90 ppm (labeled 2) (see Figure 4). The −103 ppm resonance (labeled 3) is thought to derive from an impurity phase given that its resonances are uncorrelated peaks 1 and 2. This would be consistent with the impurity observed in the X-ray Rietveld refinement. However, it should be noted that Kiczenski and Stebbins[38] list the ^{19}F NMR chemical shifts of SrF_2 and BaF_2 as −84.1 ppm and −15 ppm respectively, so the chemical shift of 3 is not necessarily consistent with $(Sr,Ba)F_2$. Interestingly, the compound $BaAlF_5$ has a chemical shift at −111 ppm, which is close to where the assigned impurity is seen. The resonance 1 (close to −73 ppm) is assigned to F substituting for O on a site that is bonded to two Sr, two Ba, and one Al, and this site is only lightly populated so that there are no 1−1 correlations. The resonance 2 at −90 ppm is assigned to F at 4*c*, densely populated give both strong 1−2 and 2−2 correlations, and close in resonance frequency to what is observed for SrF_2. At this site, the F have 4 Sr neighbors and 2 Ba neighbors. These assignments are the subject of future study.

The room temperature PL spectra of SBAF:Ce^{3+} ($x = 0$) as a function of the Ce^{3+} concentration y with 400 nm excitation are displayed in Figure 5(a). The emission spectrum is broad, with a maximum at about 460 nm arising from the transition of Ce^{3+} from the $5d^1$ excited state to the $^2F_{5/2}$ and $^2F_{7/2}$ ground states.[39] The emission spectrum displays two emission bands, at 460 nm and at 502 nm. With increasing Ce^{3+} concentration, the spectral shape changes, possibly because of changes in the subsitutional sites for the Ce atom, or energy transfer (or energy migration) between two Ce^{3+} centers, which would show strong concentration dependence. The small concentration of Ce^{3+} ions in the host lattice did not permit the quantitative determination on which substitutional sites the Ce^{3+} ions occupy via direct analytical tools. However, we can infer that Ce^{3+} ions occupy both two sites (of Sr1 and Sr2) in the lattice separately because the two emission bands of SBAF:Ce^{3+} phosphor are quite different. As described in Figure 1, the polyhedral geometry around Ce^{3+} in the lattice can be described by a completely nondegenerate set of the Ce 5d orbitals,[40] which generates two different emission energies. As shown in Figure 5(a), a decrease of the blue component around 460 nm and an increase of green around 502 nm with increasing Ce^{3+} concentration, concurrently with the emission band at 460 nm shifting to longer wavelength can be attributed to changes in the crystal field around Ce^{3+} as a result of the smaller ionic radius of Ce^{3+} (CN = 8, 1.143 Å, CN = 10, 1.25 Å) compared to Sr^{2+} (CN = 8, 1.26 Å, CN = 10, 1.36 Å).[41] In particular, for the emission spectra of $y = 0.03$, the green component around 502 nm dominates. The quantum efficiency of the optimal samples of Sr_3AlO_4F:Ce^{3+} [SBAF:Ce^{3+} ($x = 0$)] was measured to be close to 83% at room temperature.

The dependence of peak position and emission intensity on Ce^{3+} substitution are displayed in panels (b) and (c) of Figure 5. The optimum Ce^{3+} concentration was found to be 0.025, from which it is possible to calculate the critical distance (R_c) for concentration quenching. In this case, the critical distance is equal to the average shortest distance between the nearest activator ions corresponding to the critical concentration (X_c). This critical distance is represented:[42]

$$R_c \approx 2\left(\frac{3V}{4\pi X_c N}\right)^{1/3} \quad (1)$$

where, V is unit cell volume, and N is number of total Ce^{3+} sites per unit cell. On the basis of the structural parameters (see Table 1), we use the values $V = 511.2$ Å^3, $N = 8$, and $X_c = 0.025$. R_c is determined to be 16 Å.

We also used the Dexter formula described below to calculate R_c based on the spectral data of SBAF:Ce^{3+} ($x = 0$). The formula represents restricted transfer of electric dipole−dipole interaction, and is applicable since we deal here with dipole-allowed transitions in the case of Ce^{3+}. The probability of transfer of dipole−dipole interaction has been given by Blasse.[43]

$$R_c^6 = 0.63 \times 10^{28} \frac{4.8 \times 10^{-16} P}{E^4} \int f_S(E)\, F_A(E)\, \mathrm{d}E \quad (2)$$

(37) Feike, M.; Demco, D. E.; Graf, R.; Gottwald, J.; Hafner, S.; Spiess, H. W. *J. Magn. Reson.* **1996**, *122*, 214.
(38) Kiczenski, T. J.; Stebbins, J. F. *J. Non-Cryst. Solids* **2002**, *306*, 160.
(39) Blasse, G.; Grabmaier, B. C. *Luminescent materials*; Springer-Verlag: Berlin; New York, 1994.
(40) Rack, P. D.; Holloway, P. H. *Mater. Sci. Eng. R* **1998**, *21*, 171.
(41) Shannon, R. D. *Acta Crystallogr.* **1976**, *A32*, 751.
(42) Blasse, G. *Philips Res. Rep.* **1969**, *24*, 131.
(43) Dexter, D. L. *J. Chem. Phys.* **1953**, *21*, 836.

where P is the oscillator strength of the Ce^{3+} ion, E is the energy of maximum spectral overlap, and the integral represents spectral overlap, which is the product of normalized spectral shapes of emission and excitation. The values of E and $\int f_s(E)\, F_A(E)\, dE$ can be derived from the spectral data in Figure 5(a), and are 2.8 eV and 2.8×10^{-2} eV^{-1}, respectively. For P corresponding to the broad 4f ↔ 5d absorption band, a value of 10^{-2} is taken from Blasse.[43] From the eq 2, the value of R_c for the energy transfer in SBAF:Ce^{3+} was calculated as 15 Å, which is close to the value of 16 Å obtained using the concentration quenching data.

The difference of excitation and emission position between SBAF:Ce^{3+} and LSA:Ce^{3+} are discussed by means of change in the Ce^{3+}-ligand covalency from the substitution of F^- for O^{2-}. The position of [Xe]$5d^1$ configuration of Ce^{3+} can be predicted within various host lattices, which has been studied systematically by Dorenbos, and described parametrically with anion polarizability and cation electronegativity.[44−47] The position of the 5d band is mainly influenced by two factors: the centroid shift (ε_c) and the crystal field splitting (ε_{cfs}). Basically the ε_c is associated with the nephelauxetic effect, which is attributed to the interaction between 5d electron cloud and ligand ions. The latter contribution, ε_{cfs}, is determined by the shape and size of the polyhedron. Thus, the main contributions in the difference of their optical properties in the phosphors are correlated to the ε_c associated with anion polarizability and cation electronegativity because of their being isostructural. The 5d centroid shift can be estimated by taking into account the average anion electronegativity combined with Ce^{3+}−O^{2-} (or F^-) bond lengths, obtained here from the Rietveld refinement.[see Table 2] The model describes the correlated motion between 5d electron and ligand electrons as described in the following expression:[46,47]

$$\varepsilon_c = 1.79 \times 10^{13} \sum_{i=1}^{N} \frac{\alpha_{sp}^{i}}{(R_i - 0.6\Delta R)^6} \qquad (3)$$

where

$$\alpha_{sp}^{O} = 0.33 + \frac{4.8}{\chi_{av}^2} \qquad (4)$$

and

$$\alpha_{sp}^{F} = 0.15 + \frac{0.96}{\chi_{av}^2} \qquad (5)$$

Here R_i is the distance (pm) between Ce^{3+} and anion i in the lattice, α_{sp} is the spectroscopic polarizability, ΔR is the difference in ionic radii for La^{3+}/Ce^{3+} and Sr^{2+} (or Ba^{2+})/Ce^{3+}, and χ_{av} is the average cation electronegativity for nonbinary compounds containing different

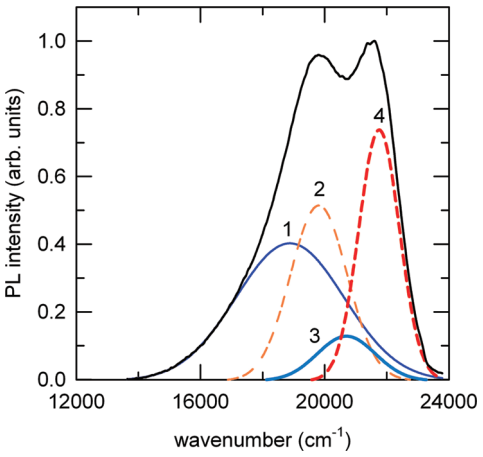

Figure 6. PL emission spectra of $Sr_{1.975}BaCe_{0.025}AlO_4F$ (x = 1.0) at 77 K. Assuming Ce ions occupy both Sr and Ba sites in the host lattice, the emission spectrum is analyzed by peak deconvolution of Gaussian components, where 1, 3 indicates Ce substituting for $Sr1O_6F_2$ and 2, 4 indicated for the substitution of $Ba1O_8F_2$.

cations. Using eqs 3−5, the centroid shifts are determined to be 14000 cm^{-1}, and 5000 cm^{-1} for LSA:Ce^{3+} and SBAF:Ce^{3+} (x = 1.0), respectively. In particular, the calculated value of centroid shift for LSA:Ce^{3+} is close to the value obtained for YAG:Ce^{3+}.[24] Thus, the energy difference in emission and excitation difference between the two phosphors are strongly accounted for the centroid shift as described in the nature and composition of the coordination polyhedra around Ce^{3+}.

From the variation of emission spectra with Ce^{3+} concentration, as well as low temperature PL measurement at 77 K, we confirm that Ce^{3+} ions occupy both Sr and Ba sites, generating two peaks in the PL spectra [see Figure 5(a) and Figure 7]. Basically the Ce^{3+} ion, $4f^1$ ground state configuration of $^2F_{5/2}$ and $^2F_{7/2}$, yields two levels whose maxima are separated by 1600 cm^{-1} to 2000 cm^{-1} because of spin−orbit coupling.[39] Thus, the emission band of the SBAF:Ce^{3+} (x = 1.0) was deconvoluted into two or four Gaussians, corresponding to single and two sites for Ce^{3+} ions. Consequently using the four Gaussians for deconvolution of the emission peak obtained a reasonable value of the fitting as shown in Figure 6. Therefore, to verify the substitutional site of Ce^{3+} for each Sr site, determination of the Ce^{3+} substitutional site was carried out using the an empirical method as described in what follows.[48] The emission position of Ce^{3+} has a strong dependence on its local environment, which has been suggested to obey the relation suggested by van Uitert:[48]

$$E(\mathrm{cm}^{-1}) = Q^*\left[1 - \left(\frac{V}{4}\right)^{1/V^*} \times 10^{-(n^* E_a r^*)/80}\right] \qquad (6)$$

Here E is the position for the Ce^{3+} emission peak, Q^* is the position in energy for the lower d-band edge for the free Ce^{3+} ion (Q^* = 50000 cm^{-1}), V^* is the valence of the Ce^{3+} ion (V^* = 3), n^* is the number of anions in the immediate shell about the Ce^{3+} ion, E_a is the electron

(44) Dorenbos, P. *Phys. Rev. B* **2000**, *62*, 15640.
(45) Dorenbos, P. *Phys. Rev. B* **2001**, *64*, 12.
(46) Dorenbos, P. *Phys. Rev. B* **2002**, *65*, 235110.
(47) Dorenbos, P. *J. Lumin.* **2003**, *105*, 117.
(48) van Uitert, L. G. *J. Lumin.* **1984**, *29*, 1.

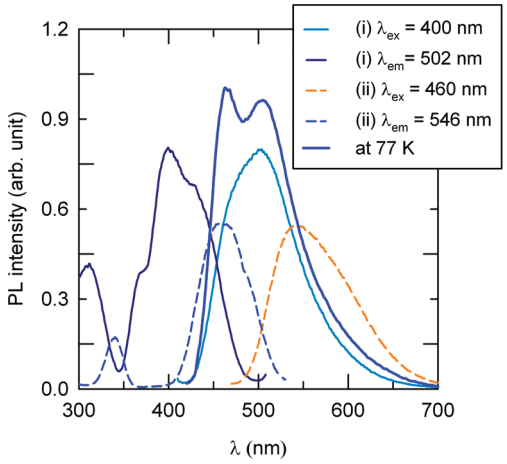

Figure 7. Excitation and emission spectra of (i) SBAF:Ce^{3+} (x = 1.0) at room temperature compared with a (ii) commercial YAG:Ce^{3+} phosphor. The PL emission spectra of SBAF:Ce^{3+} (x = 1.0) at 77 K is also displayed.

affinity of anion atom in eV, and r^* is the radius of the host cation replaced by the Ce^{3+} ion (Å). Although both are strong evidence of a Ce^{3+} center with a different local environment versus the main Ce^{3+} center in the SBAF host, it might be difficult to assign the exact nature of this lower energy Ce^{3+} center. For example, any disorder and/or charge compensation can change the local environment around specific Ce^{3+} ions, thereby modifying the position of the 4f → 5d transition. However, at least we can infer qualitatively that the emission deconvoluted into the four Gaussians comes from the $Sr1O_6F_2$ and $Ba1O_8F_2$ polyhedra. For Ce^{3+}, substituting $Sr1O_6F_2$ and $Ba1O_8F_2$, the values of V^* and E_a in eq 6 are roughly the same except for the n^*, r^*. Thus, the expected value of E calculated by the equation for $Sr1O_6F_2$ is smaller than that of Ce^{3+} in $Ba1O_8F_2$ polyhedra. Under an assumption that peak position is determined by the two Sr sites of the host lattice, the analysis of the emission spectrum by peak deconvolution into Gaussian components as shown in Figure 6 suggests $Sr1O_6F_2$ polyhedra resulted in 1, 3 components and 2, 4 for $Ba1O_8F_2$ polyhedra. The values of spin−orbit coupling were 1800 cm^{-1} and 1900 cm^{-1} for 1, 3 and 2, 4, respectively.

Figure 7 shows the PL excitation and emission spectra of SBAF:Ce^{3+} (x = 1.0) at room temperature. The results shown here suggest a PL intensity (λ_{ex} = 400 nm) that is about 150% that of commercial YAG:Ce^{3+} (λ_{ex} = 460 nm, P46-Mitsubishi Chem.) when the data are acquired under similar conditions. The value of the quantum efficiency in SBAF:Ce^{3+} (x = 1) was measured to be around 95% at room temperature. To the best of our knowledge, this is one of the highest QE values reported for a bulk phosphor sample under a long UV excitation. Compared with LSA:Ce^{3+},[27] SBAF:Ce^{3+} with x = 1.0 is twice as efficient in terms of quantum efficiency. The only difference between these phosphors from a structural viewpoint is in the polyhedral geometry, which includes F ions in the oxyfluorides [see Figure 1]. One suggestion for why the fluorine substitution results in such vast increase in the quantum efficiency is revealed by low-temperature (77 K) measurements of the

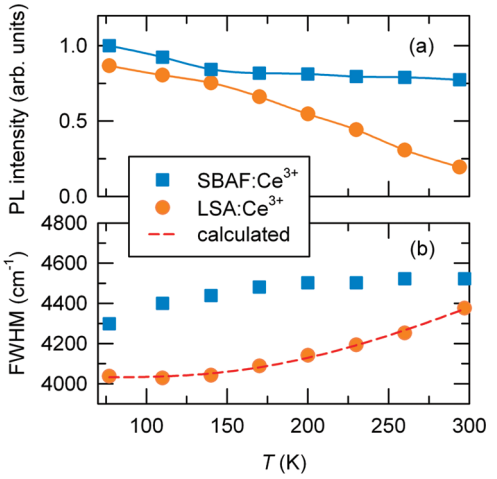

Figure 8. (a) Temperature dependent PL intensity of $La_{0.975}Ce_{0.025}Sr_2AlO_5$ and $Sr_{1.975}BaCe_{0.025}AlO_4F$ [SBAF:Ce^{3+} (x = 1.0)] in the range from 77 to 298 K. The PL of the phosphors were measured under 457 and 405 nm excitation, respectively, since these compounds have distinct excitation maxima. (b) Full width at half-maximum as a function of temperature. The dashed lined for $La_{0.975}Ce_{0.025}Sr_2AlO_5$ shows the best fitting to the eq 7.

quantum efficiency of the title compound compared with the oxide LSA:Ce^{3+}: there appears to be considerable thermal quenching in the oxide between 77 K and room temperature (RT), whereas the extent of such quenching in the oxyfluoride is greatly decreased. Figure 8 (a) shows the PL behavior of LSA:Ce^{3+} and SBAF:Ce^{3+} (x = 1.0) in the temperature range from 77 to 298 K. While SBAF:Ce^{3+} (x = 1.0) almost maintains the initial value of PL up to RT, the LSA:Ce^{3+} emission intensity decreases by about 70%. This striking difference possibly arises from the softer phonon modes associated with fluorine atoms in the host lattice.

To confirm the effect of fluoine addition, we investigated the temperature variation data of full widths at half-maximum (fwhm) of the emission spectra. These can sometimes be described within the configuration coordinate diagram according to the following equation:[49−51]

$$\mathrm{FWHM}(T) = \sqrt{8 \ln 2 S}\hbar\omega \sqrt{\coth \frac{\hbar\omega}{2k_B T}} \qquad (7)$$

where $\hbar\omega$ is the mean phonon energy, S the Huang−Rhys−Pekar parameter which characterizes electron−phonon interactions, and k_B is the Boltzmann constant. In general, phosphors suffer a decline in conversion efficiency as the temperature increases as a result of an increase in the nonradiative transition probability in the CCD.[39] Therefore, the fwhm of the emission spectra is affected by thermally active phonon modes. The fwhm of both the SBAF:Ce^{3+} and LSA:Ce^{3+} are displayed in Figure 8 (b). In principal, at higher temperatures the

(49) Wang, H.; Medina, F. D.; Liu, D. D.; Zhous, Y.-D. *J. Phys.: Condens. Matter* **1994**, *6*, 5373.
(50) Mikhailik, V. B.; Kraus, H.; Wahl, D.; Itoh, M.; Koike, M.; Bailiff, I. K. *Phys. Rev. B* **2004**, *69*, 9.
(51) Shionoya, S.; Yen, W. M. *Phosphor Handbook*; CRC Press: New York, 1998.

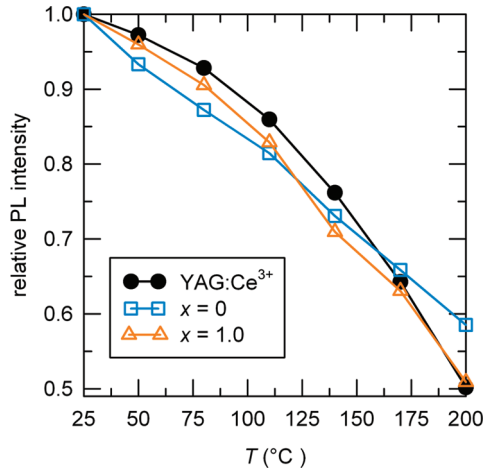

Figure 9. PL intensities for thermal quenching of commercial YAG:Ce^{3+}, $Sr_{2.975}Ce_{0.025}AlO_4F$ ($x = 0$), and $Sr_{1.975}BaCe_{0.025}AlO_4F$ ($x = 1.0$) in the temperature range from 25 to 200 °C.

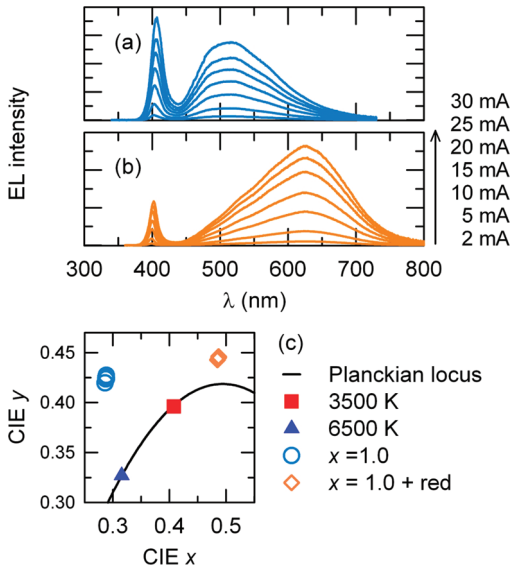

Figure 10. Luminescence of the InGaN LED + phosphor, under different forward bias currents (indicated): (a) InGaN (λ_{max} = 405 nm) + SBAF:Ce^{3+} ($x = 1.0$), (b) InGaN (λ_{max} = 405 nm) + SBAF:Ce^{3+} ($x = 1.0$) + commercial red phosphor. (c) CIE chromaticity coordinates of the device under different forward bias currents [as in panel (a) and (b)]. The Planckian locus line and the points corresponding to color temperatures of 3500 and 6500 K are indicated.

population density of phonons is increased, and the electron−phonon interaction is dominant, which results in broadening the emission spectrum as shown in Figure 8 (b). By fitting eq 7, the best fit to the emission of LSA:Ce^{3+} was obtained with Huang−Rhys−Pekar parameter $S = 11$ and phonon energy $\hbar\omega = 520\ cm^{-1}$. It is reported that YAG:Ce^{3+} shows $S = 6$ and $\hbar\omega = 200\ cm^{-1}$.[52] These results support the much stronger thermal quenching of LSA:Ce^{3+}, with a 50% loss of PL intensity at 200 °C (see Figure 9). SBAF:Ce^{3+}, however, does not fit well using eq 7 because this equation can be used only when the parabolas of the ground state and the excited state have the same curvature.[49] As we described in Figure 7, SBAF:Ce^{3+} displays multipeak emission associated with two substitution sites and energy migration within the crystal structure, curve fitting using eq 7 does not work well. Nevertheless, the fwhm of SBAF:Ce^{3+} in the range from 104 to 111 nm is much narrower than that of LSA:Ce^{3+} in the range from 143 to 150 nm, suggesting that SBAF:Ce^{3+} more closely resembles YAG:Ce^{3+} in terms of the phonon modes than it does LSA:Ce^{3+}, and hence the enhanced quantum efficiency on going from the fluoride to the oxyfluoride.

Figure 9 shows temperature quenching characteristics of commercial YAG:Ce^{3+}, SBAF:Ce^{3+} ($x = 0$), and SBAF:Ce^{3+} ($x = 1.0$) in the temperature range from 25 to 200 °C. The oxyfluorides are nearly as good as YAG:Ce^{3+} in terms of their thermal quenching properties, and beyond 170 °C, SBAF:Ce^{3+} ($x = 1.0$) is possibly even better. The introduction of F ions into the oxide host lattice can decrease the extent of thermal quenching of the phosphor during LED operation as a consequence of the softer phonon modes.

It has been reported that halide and alkali metal ion in phosphors are detrimental to moisture resistance.[53] Indeed, the main drawback of SBAF:Ce^{3+} is that it degrades upon contact with moisture. However, the SBAF:Ce^{3+} phosphors are air stable, in agreement with the previous report[29] on this compound. Preparing and processing in dry conditions and encapsulating the particles[54,55] could eliminate the moisture sensitivity.

Figure 10 (a) shows electroluminescence spectra from a device fabricated with the SBAF:Ce^{3+} phosphor ($x = 1.0$) on an InGaN LED (λ_{max} = 405 nm) under different forward bias currents in the range of 2 mA to 30 mA as indicated. The measured luminous efficacy was 10 lm/W to 15 lm/W depending on the current. These numbers reflect the low efficiency of the InGaN LED dies used here, and not the phosphor itself.

A color rendering index (R_a) is one of the most important values to evaluate the performance of white LEDs. R_a is a quantitative measure of the ability of a light source to reproduce various colors found on typical objects as compared to the colors that are observed when the lighting source is a perfect blackbody.[56] For example, conventional white LEDs with YAG:Ce^{3+} phosphor pumped by a blue LED have R_a values in the range from 70 to 75. From observed CIE chromaticity coordinates (0.28, 0.42) and color temperature 6900 K at 20 mA, we obtain R_a of about 62. Through the addition of proprietary red components in the phosphor, the R_a value of the LED could be improved to 87 as shown in Figure 10(b). Given that overall white LED performance is strongly dependent on numerous parameters starting with the external quantum efficiency of the LED chip, ratio of

(52) Bachmann, V.; Ronda, C.; Meijerink, A. *Chem. Mater.* **2009**, *21*, 2077.
(53) Ropp, R. C. *Luminescence and the Solid State*; Elsevier: Amsterdam, 1991.
(54) Im, W. B.; Yoo, H. S.; Vaidyanathan, S.; Kwon, K. H.; Park, H. J.; Kim, Y.-I.; Jeon, D. Y. *Mater. Chem. Phys.* **2009**, *115*, 161.
(55) Avci, N.; Musschoot, J.; Smet, P. F.; Korthout, K.; Avci, A.; Detavernier, C.; Poelmana, D. *J. Electrochem. Soc.* **2009**, *156*, J333.
(56) Schubert, E. F. *Light-emitting diodes*, 2nd ed.; Cambridge University Press: Cambridge, 2006.

encapsulant to phosphor powder, phosphor particle size, and so forth, we anticipate that all properties in this system can be further improved.

Conclusions

We have developed a new phosphor family, $Sr_{2.975-x}Ba_xCe_{0.025}AlO_4F$, which displays unprecedented efficiency under 400 nm excitation. Compared with the oxide parent phase $LaSr_2AlO_5:Ce^{3+}$, SBAF:Ce^{3+} (x = 1.0) nearly maintains the initial PL intensity up to room temperature, which results in twice the efficiency. Applying SBAF:Ce^{3+} ($x = 1.0$) on InGaN LEDs (λ_{max} = 405 nm), we obtain white LEDs with a brightness of 13 lm/W at 20 mA. The near 100% QE of the new SBAF:Ce^{3+} phosphor suggests great potential for high luminous efficacy white LEDs as well as more efficient broad green emitters.

Acknowledgment. We thank the National Science Foundation (DMR05-20415) for use of MRSEC facilities at UCSB and the Solid State Lighting and Energy Center at UCSB for support.

Supporting Information Available: Additional information on the determination of the photoluminescence quantum efficiency (PLQE) in solid samples. This material is available free of charge via the Internet at http://pubs.acs.org.